

Crystal structure of elvitegravir Form II, C₂₃H₂₃ClFNO₅James A. Kaduk ^{1,2,a)} Stacy Gates-Rector ³ and Thomas N. Blanton ³¹Illinois Institute of Technology, 3101 S. Dearborn St., Chicago, IL 60616, USA²North Central College, 131 S. Loomis St., Naperville, IL 60540, USA³ICDD, 12 Campus Blvd., Newtown Square, PA 19073-3273, USA

(Received 18 August 2022; accepted 23 September 2022)

The crystal structure of elvitegravir Form II has been solved and refined using synchrotron X-ray powder diffraction data, and optimized using density functional theory techniques. Elvitegravir Form II crystallizes in space group $P2_1$ (#4) with $a = 11.54842(7)$, $b = 14.04367(5)$, $c = 13.33333(8)$ Å, $\beta = 90.0330(6)^\circ$, $V = 2162.427(14)$ Å³, and $Z = 4$. The crystal structure consists of alternating layers of parallel molecules perpendicular to the b -axis. The mean planes of the oxoquinoline ring systems in molecules 1 and 2 are 1(22)-1 and -1(22)1. Between the stacks are layers of the halogenated phenyl rings. These exhibit herringbone stacking. In each molecule, the carboxylic acid group forms a strong intramolecular O–H...O hydrogen bond to the nearby carbonyl group. The hydroxyl group of each molecule forms a strong hydrogen bond to the carbonyl group of the carboxylic acid of the other molecule. These O–H...O hydrogen bonds link the molecules into dimers, with a graph set $R2,2(18) > a > c$. The powder pattern has been submitted to ICDD for inclusion in the Powder Diffraction File™ (PDF®).

© The Author(s), 2023. Published by Cambridge University Press on behalf of International Centre for Diffraction Data. This is an Open Access article, distributed under the terms of the Creative Commons Attribution licence (<http://creativecommons.org/licenses/by/4.0/>), which permits unrestricted re-use, distribution and reproduction, provided the original article is properly cited. [doi:10.1017/S0885715622000501]

Key words: elvitegravir, Vitekta®, powder diffraction, Rietveld refinement, density functional theory

I. INTRODUCTION

Elvitegravir is a modified quinolone antibiotic with activity against human immunodeficiency virus 1. Elvitegravir is an inhibitor of the enzyme viral integrase and retains activity against integrase mutants that are resistant to Raltegravir (PubChem; Kim *et al.*, 2019). It was developed by the pharmaceutical company Gilead Sciences, which licensed it from Japan Tobacco in March 2008. The drug gained approval by the U.S. Food and Drug Administration on August 27, 2012 for use in adult patients starting HIV treatment for the first time as part of the fixed-dose combination known as Stribild. On September 24, 2014, the FDA approved elvitegravir as a single pill formulation under the trade name Vitekta. On November 5, 2015, the FDA approved the drug for use in patients affected with HIV-1 as a part of a second fixed-dose combination pill known as Genvoya. The systematic name (CAS Registry Number 697761-98-1) is 6-[(3-chloro-2-fluorophenyl) methyl]-1-[(2S)-1-hydroxy-3-methylbutan-2-yl]-7-methoxy-4-oxoquinoline-3-carboxylic acid. A two-dimensional molecular diagram is shown in Figure 1.

Elvitegravir and many similar compounds are claimed in US Patent 7,176,220 B2 (Satoh *et al.*, 2007; Japan Tobacco Inc.), but no X-ray powder diffraction data were provided. Crystalline Forms I, II, and I of elvitegravir are claimed in

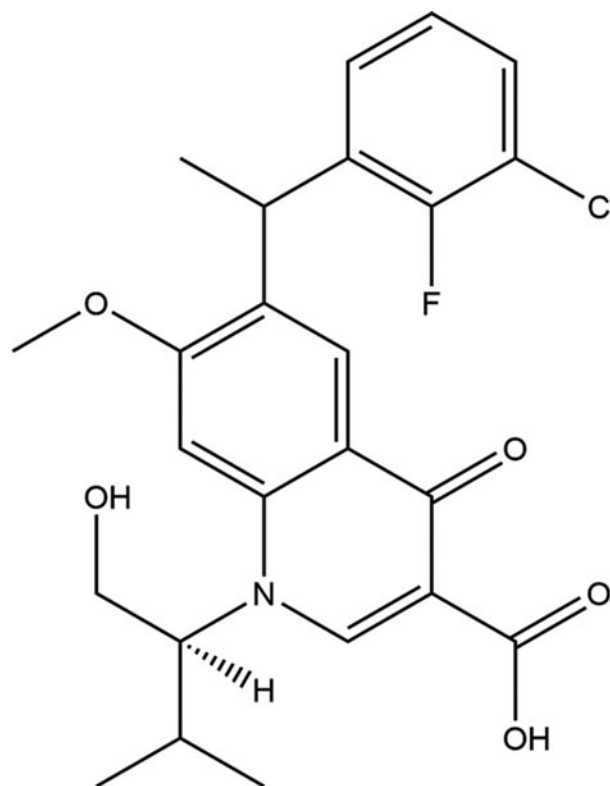


Figure 1. The 2D molecular structure of elvitegravir.

^{a)} Author to whom correspondence should be addressed. Electronic mail: kaduk@polycrystallography.com

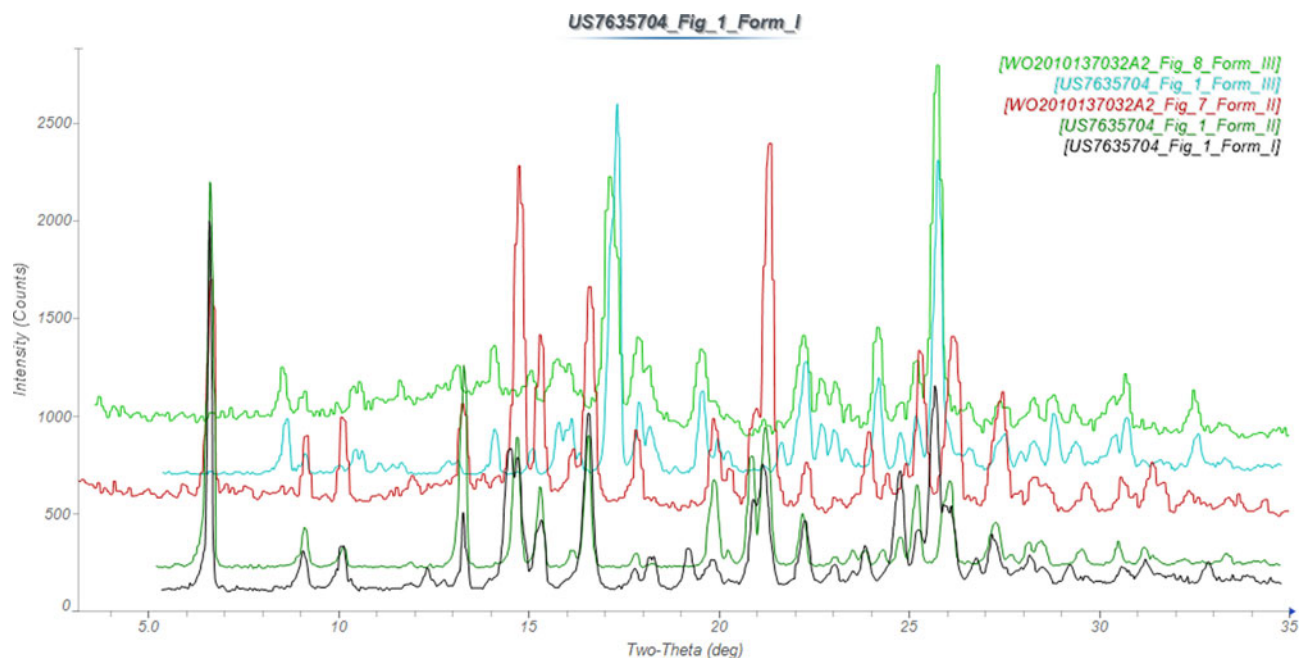


Figure 2. Comparison of the X-ray powder diffraction patterns of elvitegravir Forms I, II, and III from Satoh *et al.* (2009) and Vellanki *et al.* (2010). The patterns were digitized using UN-SCAN-IT (Silk Scientific, 2013). Image generated using JADE Pro (MDI, 2022).

US Patent 7,635,704 B2 (Satoh *et al.*, 2009; Japan Tobacco Inc.), and XRD data are reported. Powder data for Forms II and III of elvitegravir, as well as for the amorphous form and amorphous and crystalline sodium salts, are reported in Vellanki *et al.* (2010; Matrix Laboratories Ltd.). Both Form II and Form III from both Japan Tobacco and Matrix seem to represent the same respective polymorphs (Figure 2).

This work was carried out as part of a project (Kaduk *et al.*, 2014) to determine the crystal structures of large-volume commercial pharmaceuticals, and include high-quality powder diffraction data for them in the Powder Diffraction File (Gates-Rector and Blanton, 2019).

II. EXPERIMENTAL AND REFINEMENTS

Elvitegravir was a commercial reagent, purchased from TargetMol (Lot #130053), and was used as-received. The white powder was packed into a 1.5 mm diameter Kapton capillary and rotated during the measurement at ~ 50 Hz. The powder pattern was measured at 295 K at beamline 11-BM (Antao *et al.*, 2008; Lee *et al.*, 2008; Wang *et al.*, 2008) of the Advanced Photon Source at Argonne National Laboratory using a wavelength of 0.458208(2) Å from 0.5 to 50° 2θ with a step size of 0.001° and a counting time of 0.1 s step^{-1} . The high-resolution powder diffraction data were collected using twelve silicon crystal analyzers that allow for high angular resolution, high precision, and accurate peak positions. A mixture of silicon (NIST SRM 640c) and alumina (NIST SRM 676a) standards (ratio $\text{Al}_2\text{O}_3:\text{Si} = 2:1$ by weight) was used to calibrate the instrument and refine the monochromatic wavelength used in the experiment.

The pattern was indexed using N-TREOR (Altomare *et al.*, 2013) and DICVOL06 (Louër and Boulitf, 2007) as incorporated into FOX (Favre-Nicolin and Černý, 2002) on a primitive orthorhombic cell with $a = 11.54903$, $b = 13.33241$, $c = 14.04233$ Å, $V = 2162.2$ Å³, and $Z = 4$. A

reduced cell search in the Cambridge Structural Database (Groom *et al.*, 2016) combined with the chemistry C, H, Cl, F, N, and O only yielded no hits. The space group was ambiguous, but $P2_12_1$ yielded an apparent successful solution and refinement of the structure. An elvitegravir molecule was downloaded from PubChem (Kim *et al.*, 2019) as Conformer3D_CID_5277135.sdf. It was converted to a *.mol2 file using Mercury (Macrae *et al.*, 2020). The structure was solved by Monte Carlo simulated annealing as implemented in DASH (David *et al.*, 2006). The success rate was $\sim 30\%$.

The structure solution contained a void on a twofold axis, indicated by Mercury with a probe radius of 1.2 Å. The void was located in a reasonable position to form hydrogen bonds, so a water molecule was added to the model. A Rietveld refinement of 117 variables using 24 238 observations and 81 restraints yielded the residuals $R_{\text{wp}} = 0.1399$ and $\text{GOF} = 2.14$. The largest errors in the difference plot (Figure 3) were in the intensities of many of the strong low-angle peaks, and the fit was overall disappointing. The root-mean-square (rms) Cartesian displacement between the Rietveld-refined and DFT-optimized structures was 0.341 Å (Figure 4), at the upper end of the normal range for correct structures. The space group did not account for the weak (0.6% relative intensity) 1 0 0 peak at 2.27°. While no individual measure of the quality of the fit is necessarily a “red flag”, their sum motivated concern about the correctness of the structure.

Accordingly, the symmetry was lowered to $P2_1$ (to model the 1 0 0 peak), with a re-labeling of the axes to obtain the standard setting. This means that there are two molecules in the asymmetric unit, and thus, the problem is twice as large. The structure was re-solved in $P2_1$ using DASH, and the success rate was reduced to $\sim 2\%$. (The success rate in a Monte Carlo simulated annealing run tends to decrease as the number of variables increases.) Thermogravimetric analysis (TGA) confirmed that the sample was anhydrous.

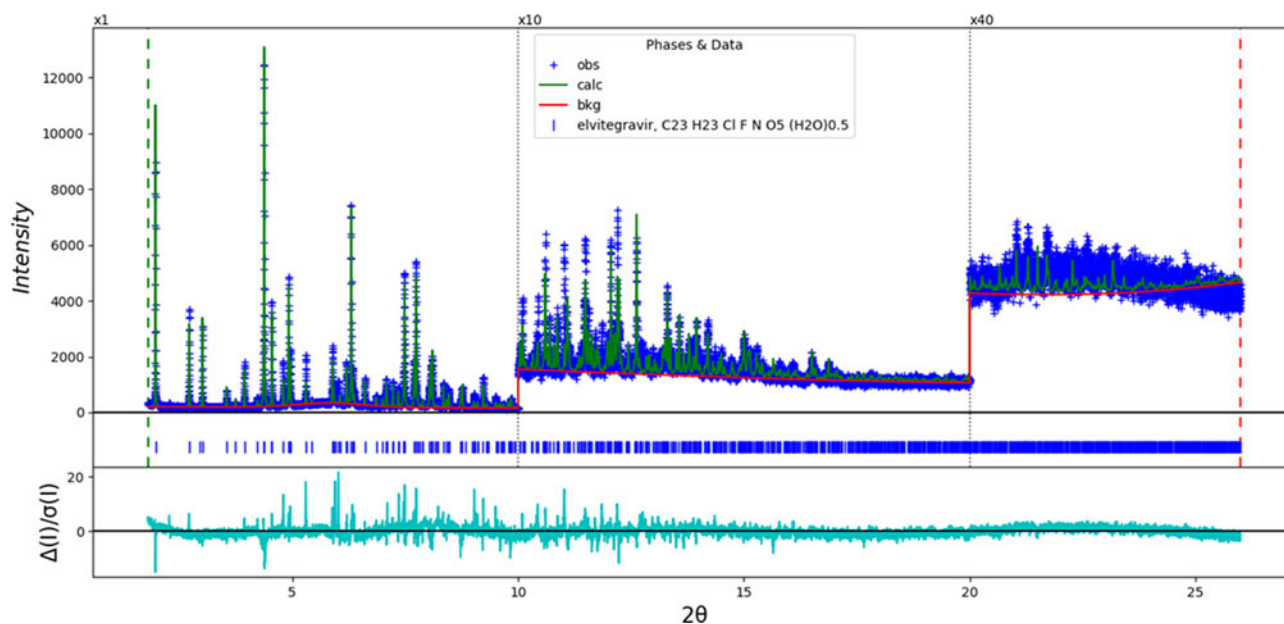


Figure 3. The Rietveld plot for the refinement of the incorrect orthorhombic structure of elvitegravir. The blue crosses represent the observed data points, and the green line is the calculated pattern. The cyan curve is the normalized error plot, and the red curve indicates the background. The vertical scale has been multiplied by a factor of 10× for $2\theta > 10.0^\circ$ and by a factor of 40× for $2\theta > 20.0^\circ$. The row of blue tick marks indicates the calculated reflection positions.

Rietveld refinement was carried out using GSAS-II (Toby and Von Dreele, 2013). Only the $1.9\text{--}24.0^\circ$ portion of the pattern was included in the refinement ($d_{\min} = 1.102 \text{ \AA}$). The y-coordinate of C11 was fixed to define the origin. There was apparently a void in the structure (Figure 5). Including an O atom (water molecule) in this void resulted in a negative occupancy, so the atom was removed. All non-H bond distances and angles (plus the planes of ring systems) were subjected to restraints, based on a Mercury/Mogul Geometry Check (Bruno *et al.*, 2004; Sykes *et al.*, 2011). The Mogul average and standard deviation for each quantity were used as the restraint parameters. The restraints contributed 9.8% to the final χ^2 . The hydrogen atoms were included in calculated positions, which were recalculated during the refinement

using Materials Studio (Dassault, 2021). The U_{iso} of the heavy atoms were grouped by chemical similarity. The U_{iso} for the H atoms were fixed at $1.3 \times U_{\text{iso}}$ of the heavy atoms to which they are attached. A second-order spherical harmonic preferred orientation model was included in the refinement. The refined texture index was 1.001(0). The peak profiles were described using the generalized microstrain model. The background was modeled using a 6-term shifted Chebyshev polynomial, and a peak at $5.79^\circ 2\theta$ to model the scattering from the Kapton capillary and any amorphous component.

The final refinement of 216 variables using 22 135 observations and 166 restraints yielded the residuals $R_{\text{wp}} = 0.0897$ and $\text{GOF} = 1.39$. The largest peak (0.11 \AA from C11) and hole (0.92 \AA from C64) in the difference Fourier map were

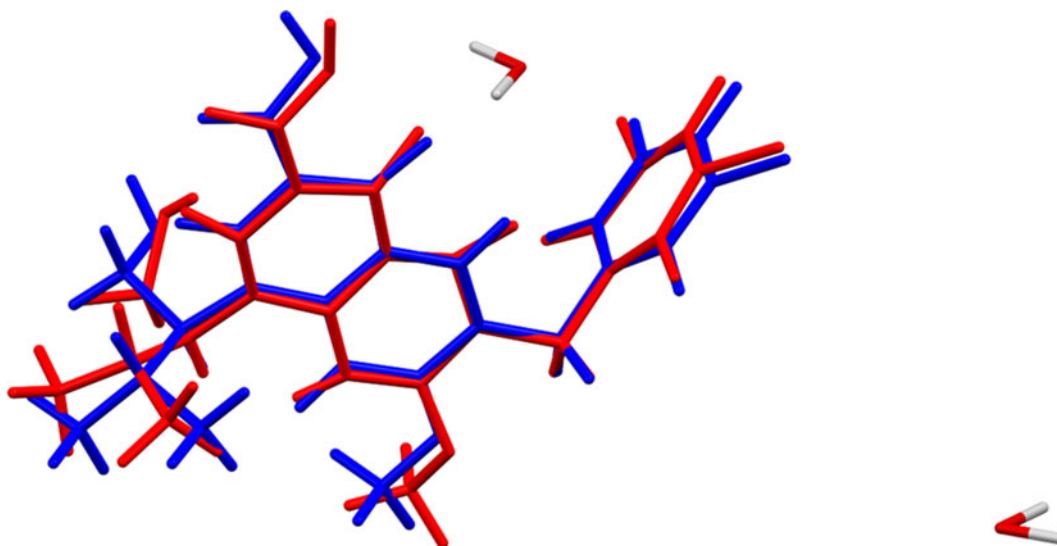
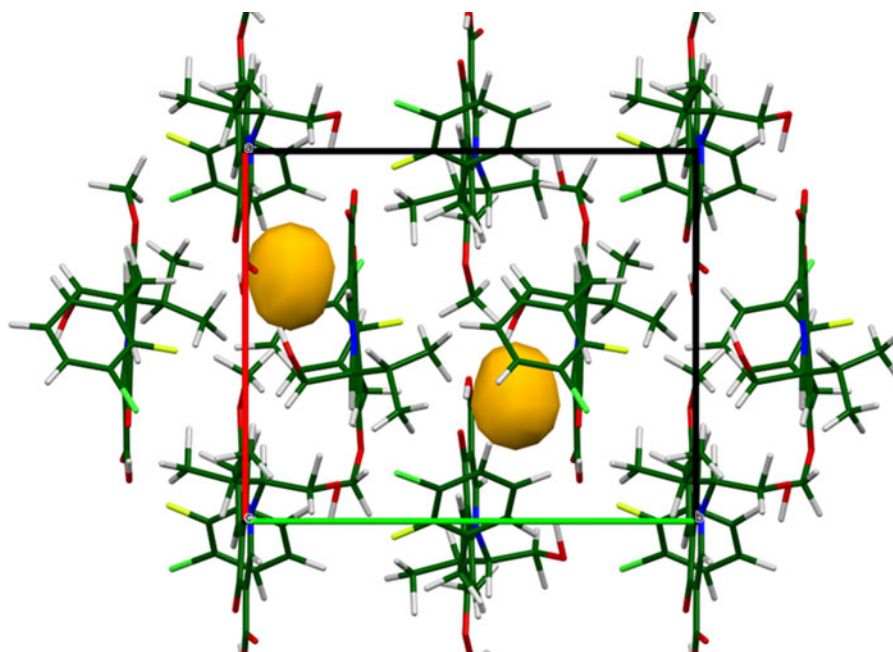


Figure 4. Comparison of the Rietveld-refined (red) and VASP-optimized (blue) structures of elvitegravir in the incorrect orthorhombic model. The rms Cartesian displacement is 0.326 \AA . Image generated using Mercury (Macrae *et al.*, 2020).



3215d Riet; r = 1.2 Ang; void goes away on DFT

Figure 5. The apparent void in the initial structure solution of the monoclinic model of elvitegravir (probe radius = 1.2 Å). Image generated using Mercury (Macrae *et al.*, 2020).

0.40(7) and $-0.27(7) e\text{\AA}^{-3}$, respectively. The largest errors in the difference plot (Figure 6) are in the shapes of some of the strong peaks and in the background, but the refinement is much more satisfactory than the first refinement.

The crystal structures were optimized using VASP (Kresse and Furthmüller, 1996) (fixed experimental unit cell) through the MedeA graphical interface (Materials Design, 2016). The calculation was carried out on 16 2.4 GHz processors (each with 4 GB RAM) of a 64-processor HP Proliant DL580 Generation 7 Linux cluster at North Central

College. The calculation used the GGA-PBE functional, a plane wave cutoff energy of 400.0 eV, and a k -point spacing of 0.5\AA^{-1} leading to a $2 \times 1 \times 1$ mesh, and took ~ 28.6 h. A single-point density functional calculation (fixed experimental cell) and population analysis were carried out using CRYSTAL17 (Dovesi *et al.*, 2018). The basis sets for the H, C, N, and O atoms in the calculation were those of Gatti *et al.* (1994), and those for F and Cl were those of Peintinger *et al.* (2013). The calculations were run on a 3.5 GHz PC using 8 k -points and the B3LYP functional,

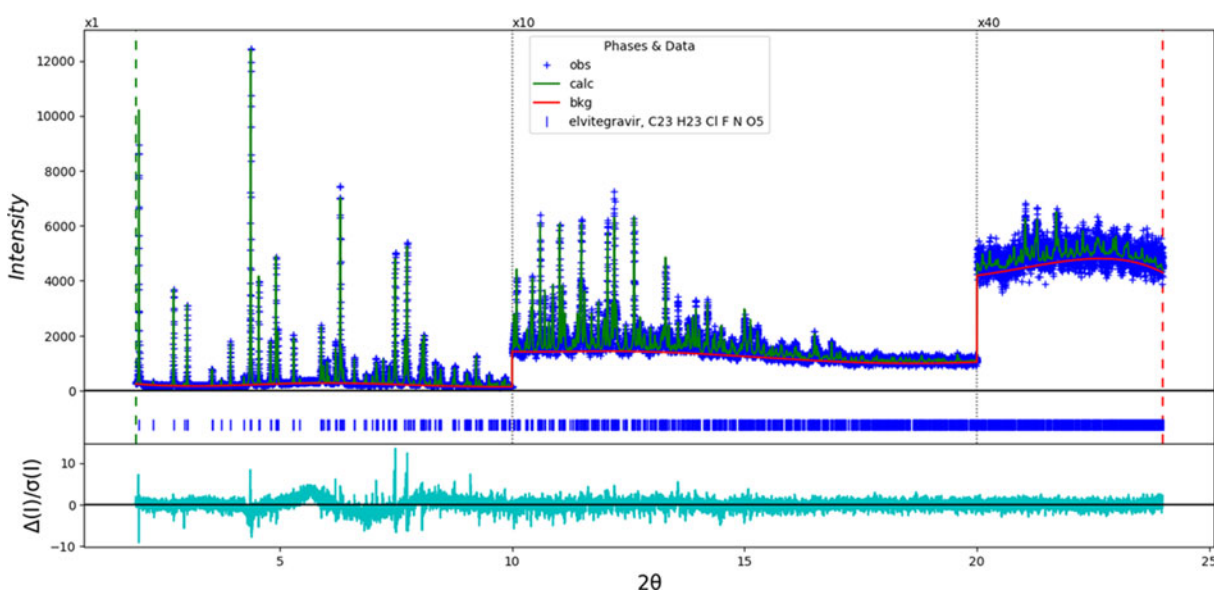


Figure 6. The Rietveld plot for the refinement of the correct monoclinic structure of elvitegravir. The blue crosses represent the observed data points, and the green line is the calculated pattern. The cyan curve is the normalized error plot, and the red curve indicates the background. The vertical scale has been multiplied by a factor of 10× for $2\theta > 10.0^\circ$ and by a factor of 40× for $2\theta > 20.0^\circ$. The row of blue tick marks indicates the calculated reflection positions.

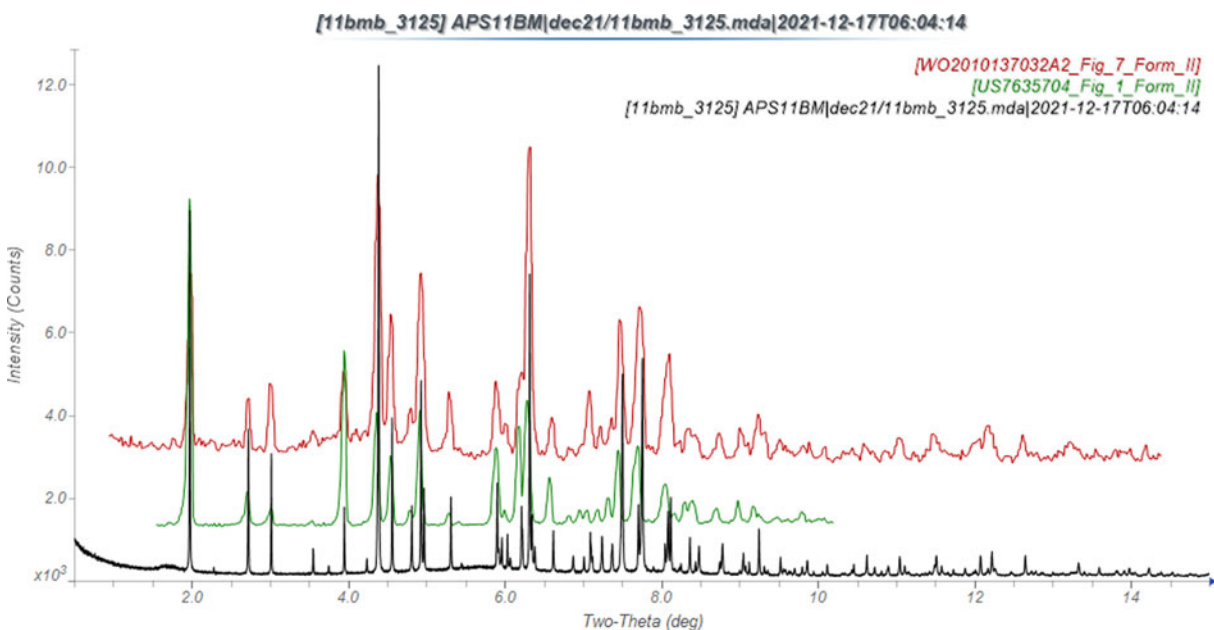


Figure 7. Comparison of the synchrotron pattern of elvitegravir (black) to that reported by Satoh *et al.* (2009; green) and Vellanki *et al.* (2010; red). The literature patterns, measured using $\text{CuK}\alpha$ radiation, were digitized using UN-SCAN-IT (Silk Scientific, 2013) and converted to the synchrotron wavelength of 0.458208 Å using JADE Pro (MDI, 2022). Image generated using JADE Pro (MDI, 2022).

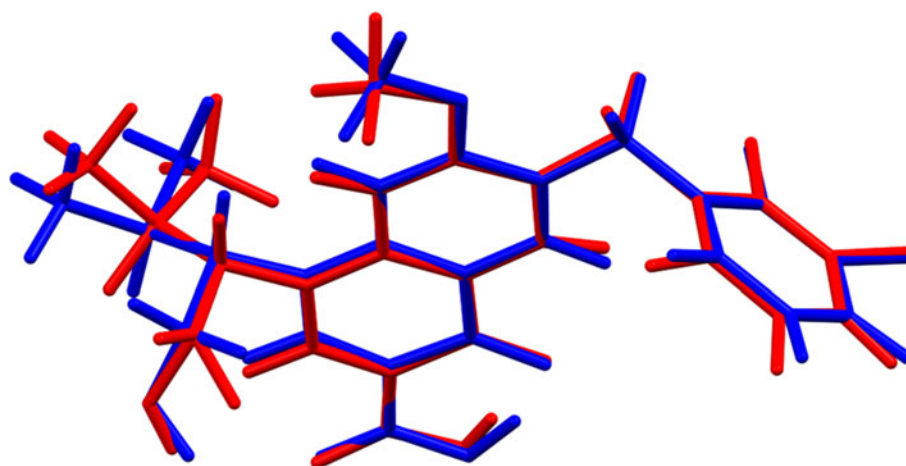
and took ~ 7.1 h. The monoclinic structure was $14.1 \text{ kcal mol}^{-1}$ lower in energy than the orthorhombic model.

III. RESULTS AND DISCUSSION

The synchrotron powder pattern of this study matches the patterns for Form II reported by Japan Tobacco (Satoh *et al.*, 2009) and Matrix (Vellanki *et al.*, 2010) well enough to conclude that our sample is elvitegravir Form II (Figure 7). The rms Cartesian displacements between the Rietveld-refined and DFT-optimized structures of elvitegravir are 0.204 and 0.129 \AA for molecules 1 (lower atom numbers) and 2 (Figures 8 and 9). The good agreement provides evidence that the structure is correct (van de Streek and Neumann,

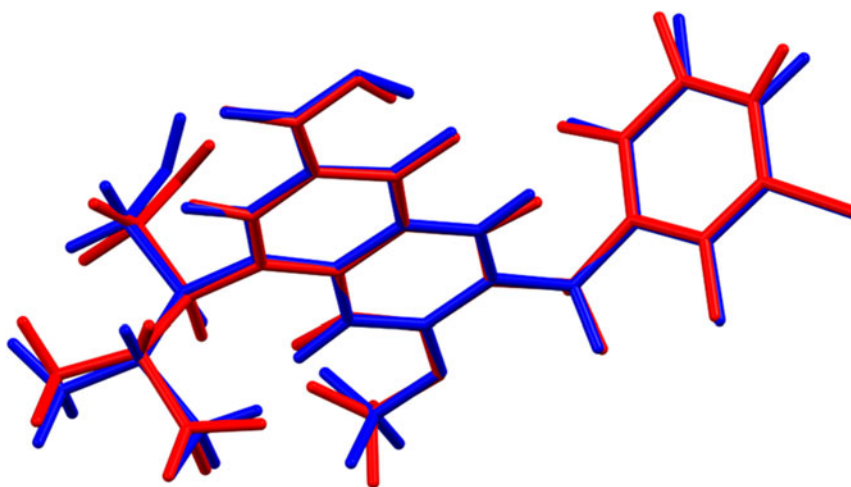
2014). The apparent void disappeared in the DFT-optimized structure. This discussion concentrates on the DFT-optimized structure. The asymmetric unit (with atom numbering) is illustrated in Figure 10. The displacement coefficients of the atoms in the isopropyl group of molecule 1 are larger than those of the other atoms, suggesting the possibility of some disorder of this group. The two independent elvitegravir molecules are similar (Figure 11), but exhibit many differences, especially in the methyl groups. The rms Cartesian displacement between the two molecules is 0.582 \AA .

The crystal structure (Figures 12 and 13) consists of alternating layers of parallel molecules perpendicular to the b -axis. The mean planes of the oxoquinoline ring systems in molecules 1 and 2 are $1(22)\text{-}1$ and $\text{-}1(22)1$. Between the stacks



Molecule 1; rmsd = 0.204

Figure 8. Comparison of the Rietveld-refined (red) and VASP-optimized (blue) structures of molecule 1 of elvitegravir. The rms Cartesian displacement is 0.204 \AA . Image generated using Mercury (Macrae *et al.*, 2020).



Molecule 2; rmsd = 0.129

Figure 9. Comparison of the Rietveld-refined (red) and VASP-optimized (blue) structures of molecule 2 of elvitegravir. The rms Cartesian displacement is 0.129 Å. Image generated using Mercury (Macrae *et al.*, 2020).

are layers of the halogenated phenyl rings. These exhibit herringbone stacking. Although the general arrangements of the molecules in the correct and incorrect structures are similar (Figure 14), there are many subtle differences.

Almost all of the bond distances, bond angles, and torsion angles fall within the normal ranges indicated by a Mercury/Mogul Geometry check (Macrae *et al.*, 2020). The C63–N62

distance of 1.495 Å (average = 1.469(7) Å, Z-score = 3.4) is flagged as unusual. The uncertainty on this average is exceptionally small, inflating the Z-score. The C10–C9–N8–C11 torsion angle is flagged as unusual. This lies within a broad distribution of a small number of similar torsion angles, and is not of concern. The torsion angles involving rotation about the C19–C23 bond lie on the tails of distributions

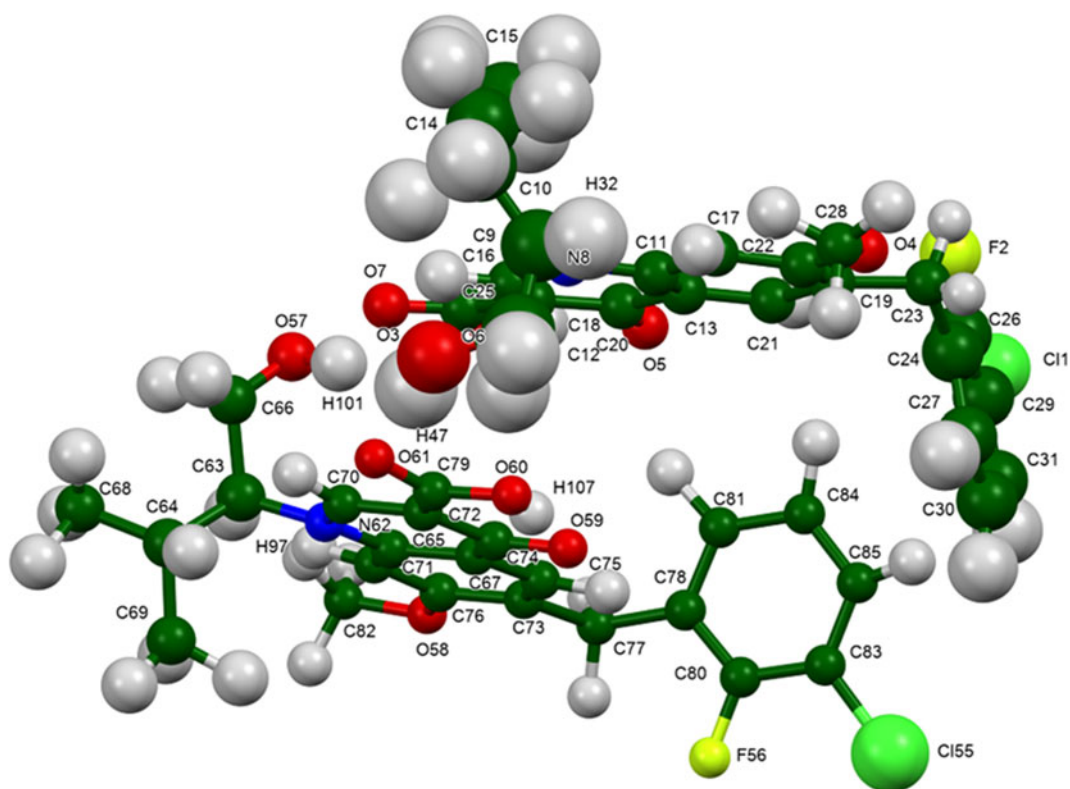
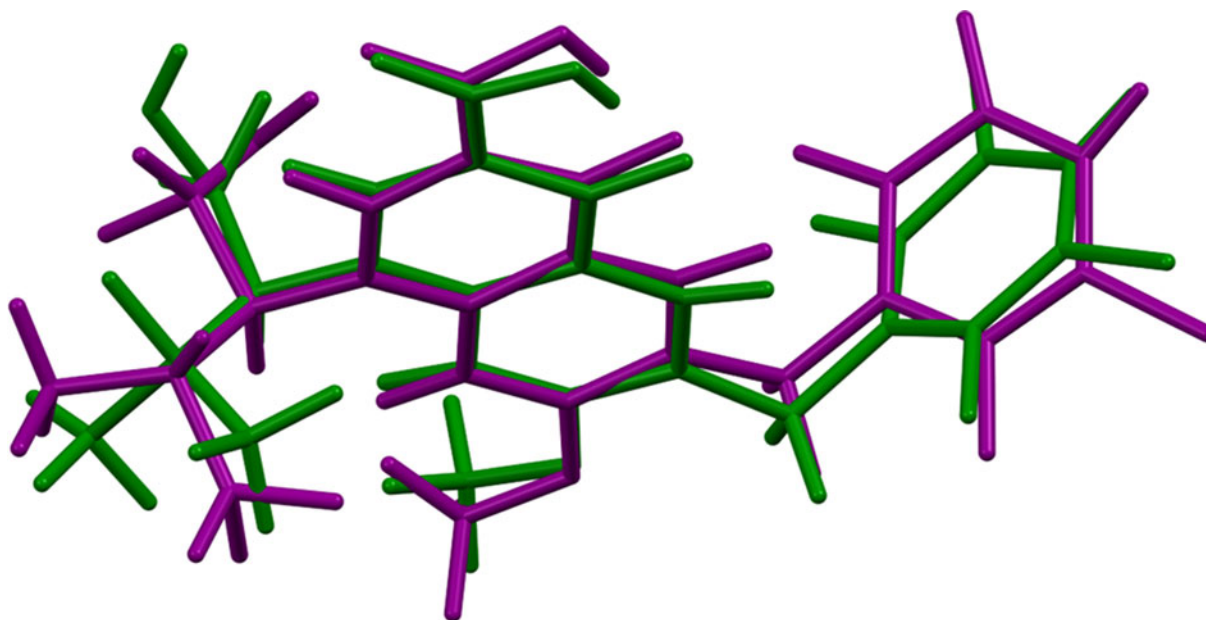


Figure 10. The asymmetric unit of elvitegravir, with the atom numbering. The atoms are represented by 50% probability spheroids. Image generated using Mercury (Macrae *et al.*, 2020).



1 green; 2 purple; rmsd = 0.582

Figure 11. Comparison of molecule 1 (green) and molecule 2 (purple) of elvitegravir. The rms Cartesian displacement is 0.582 Å. Image generated using Mercury (Macrae *et al.*, 2020).

which peak around 90°. These angles lie in the linkage between the two ring systems, and indicate that the conformation of the molecule is slightly unusual.

The quantum chemical geometry optimization of the elvitegravir molecules (DFT/B3LYP/6-31G*/water) using Spartan '18 (Wavefunction, 2020) indicated that the observed solid-state conformations are comparable in energy. The

conformational differences are small and spread throughout the molecules. A conformational analysis (MMFF force field) indicates that the global minimum-energy conformation has a similar general shape to the observed conformations, but with many small differences. The rms Cartesian displacements between molecules 1 and 2 and the global minimum-energy conformation are 1.259 and 1.270 Å, respectively. Notably,

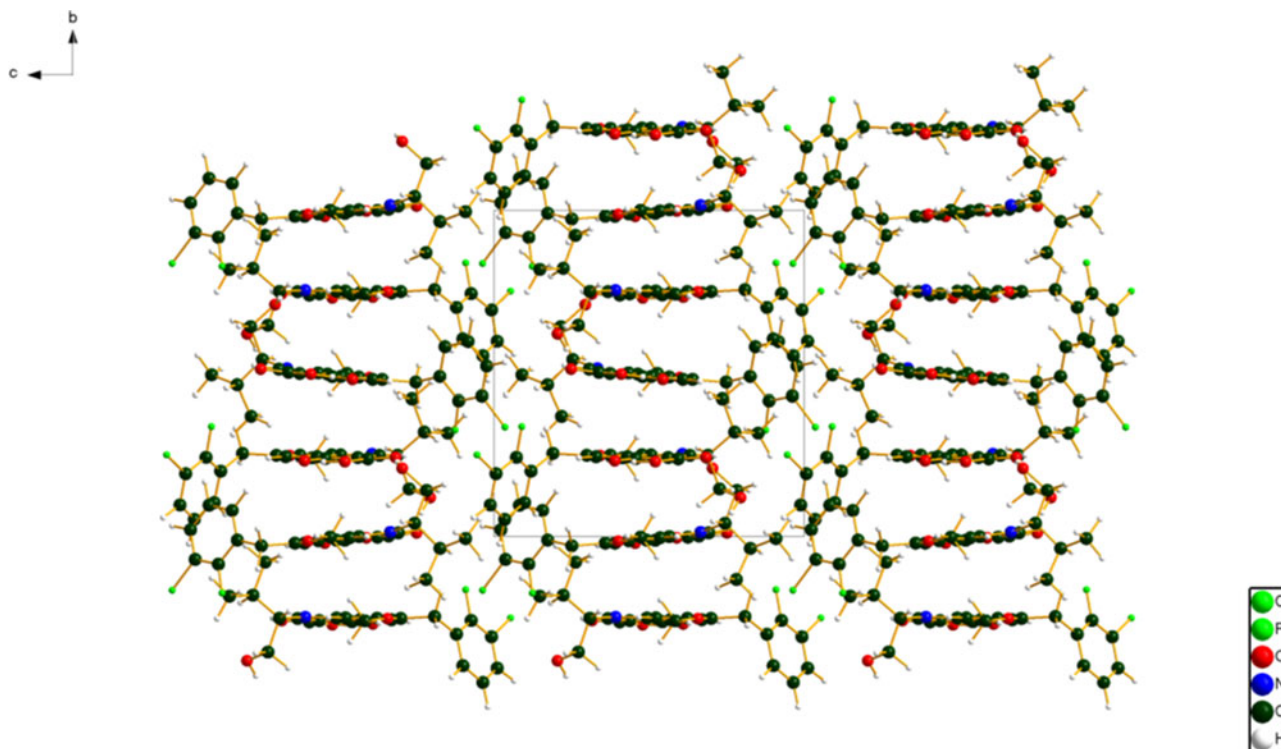


Figure 12. The crystal structure of elvitegravir, viewed down the *a*-axis. Image generated using Diamond (Crystal Impact, 2022).

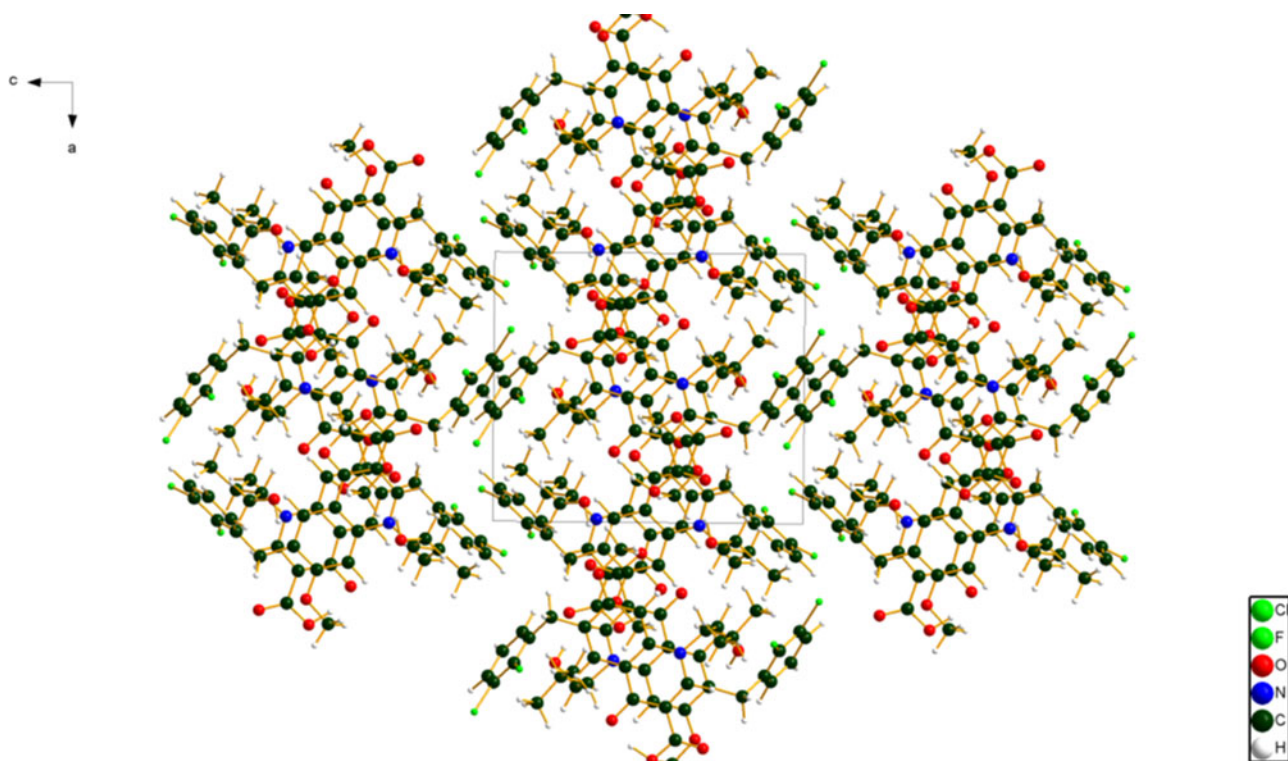


Figure 13. The crystal structure of elvitegravir, viewed down the *b*-axis. Image generated using Diamond (Crystal Impact, 2022).

the orientation of the carboxylic acid group differs in the global minimum; it does not form the intramolecular hydrogen bonds observed in the solid state.

Analysis of the contributions to the total crystal energy of the structure using the Forcite module of Materials Studio (Dassault, 2021) suggests that bond, angle, and torsion distortion terms are about equally important in the intramolecular deformation energy. The intermolecular energy is dominated by van der Waals repulsions and electrostatic attractions, which in this force field analysis include hydrogen bonds. The hydrogen bonds are better analyzed using the results of the DFT calculation.

In each molecule, the carboxylic acid group forms a strong intramolecular O–H...O hydrogen bond to the nearby carbonyl group (Table I). The energies of the O–H...O hydrogen bonds were calculated using the correlation of Rammohan and Kaduk (2018). The hydroxyl group of each molecule forms a strong hydrogen bond to the carbonyl group of the carboxylic acid of the other molecule. These O–H...O hydrogen bonds link the molecules into dimers, with a graph set (Etter, 1990; Bernstein *et al.*, 1995; Shields *et al.*, 2000) $R2,2(18) > a > c$ (Figure 15). In each molecule, two aromatic C–H form intramolecular hydrogen bonds to carbonyl O atoms.

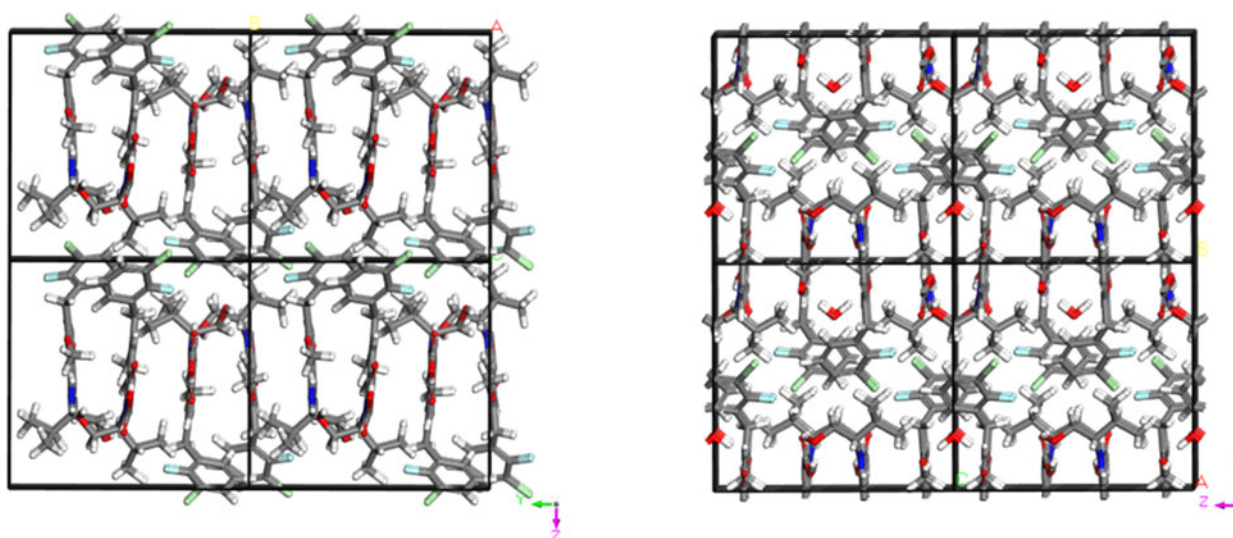


Figure 14. Comparison of the correct monoclinic (left) and incorrect orthorhombic (right) structures of elvitegravir. Image generated using Materials Studio (Dassault, 2021).

TABLE I. Hydrogen bonds (CRYSTAL17) in elvitegravir.

H-Bond	D-H (Å)	H...A (Å)	D...A (Å)	D-H...A (°)	Overlap (<i>e</i>)	E (kcal mol ⁻¹)
O6–H53...O5O60–H107...O59	1.0841.081	1.390 ^a 1.410 ^a	2.4352.451	159.5159.4	0.1200.117	18.918.7
O3–H47...O61O57–H101...O7	0.9950.995	1.7461.780	2.7002.758	159.4166.7	0.0550.056	12.812.9
C16–H42...O7C70–H96...O61	1.0891.089	2.578 ^a 2.532 ^a	2.8712.849	94.295.4	0.0130.014	
C21–H44...O5C75–H98...O59	1.0911.091	2.437 ^a 2.479 ^a	2.8102.838	98.397.6	0.0150.015	
C14–H41...O59	1.100	2.425	3.504	166.5	0.014	
C15–H39...O58C69–H93...O5	1.0971.099	2.5632.967	3.6383.273	166.296.2	0.0110.000	
C31–H54...O61	1.089	2.563	3.526	147.0	0.013	
C14–H36...C155C68–H90...C11	1.0981.099	3.0883.015	3.4294.082	98.6163.9	0.0020.010	
C23–H46...O61C77–H100...O7	1.1031.101	2.7512.453	3.6883.346	142.5137.3	0.0100.014	
C84–H106...C11	1.090	2.845	3.710	136.3	0.010	

Top line = molecule 1, and bottom line = molecule 2.

^aIntramolecular.

There are subtle differences among the C–H...O and C–H...Cl hydrogen bonds in the two molecules.

The volume enclosed by the Hirshfeld surface of elvitegravir (Figure 16; Hirshfeld, 1977; Turner *et al.*, 2017) is 1070.74 Å³, 99.03% of 1/2 the unit cell volume. The packing density is thus fairly typical. The only significant close contacts (red in Figure 16) involve the hydrogen bonds. The volume/non-hydrogen atom is typical at 16.9 Å³.

The Bravais–Friedel–Donnay–Harker (Bravais, 1866; Friedel, 1907; Donnay and Harker, 1937) morphology suggests that we might expect blocky morphology for

elvitegravir. A second-order spherical harmonic preferred orientation model was included in the refinement. The texture index was 1.001(0), indicating that preferred orientation was not significant for this rotated capillary specimen.

IV. DEPOSITED DATA

The powder pattern of elvitegravir from this synchrotron data set has been submitted to ICDD for inclusion in the Powder Diffraction File. The Crystallographic Information Framework (CIF) files containing the results of the Rietveld

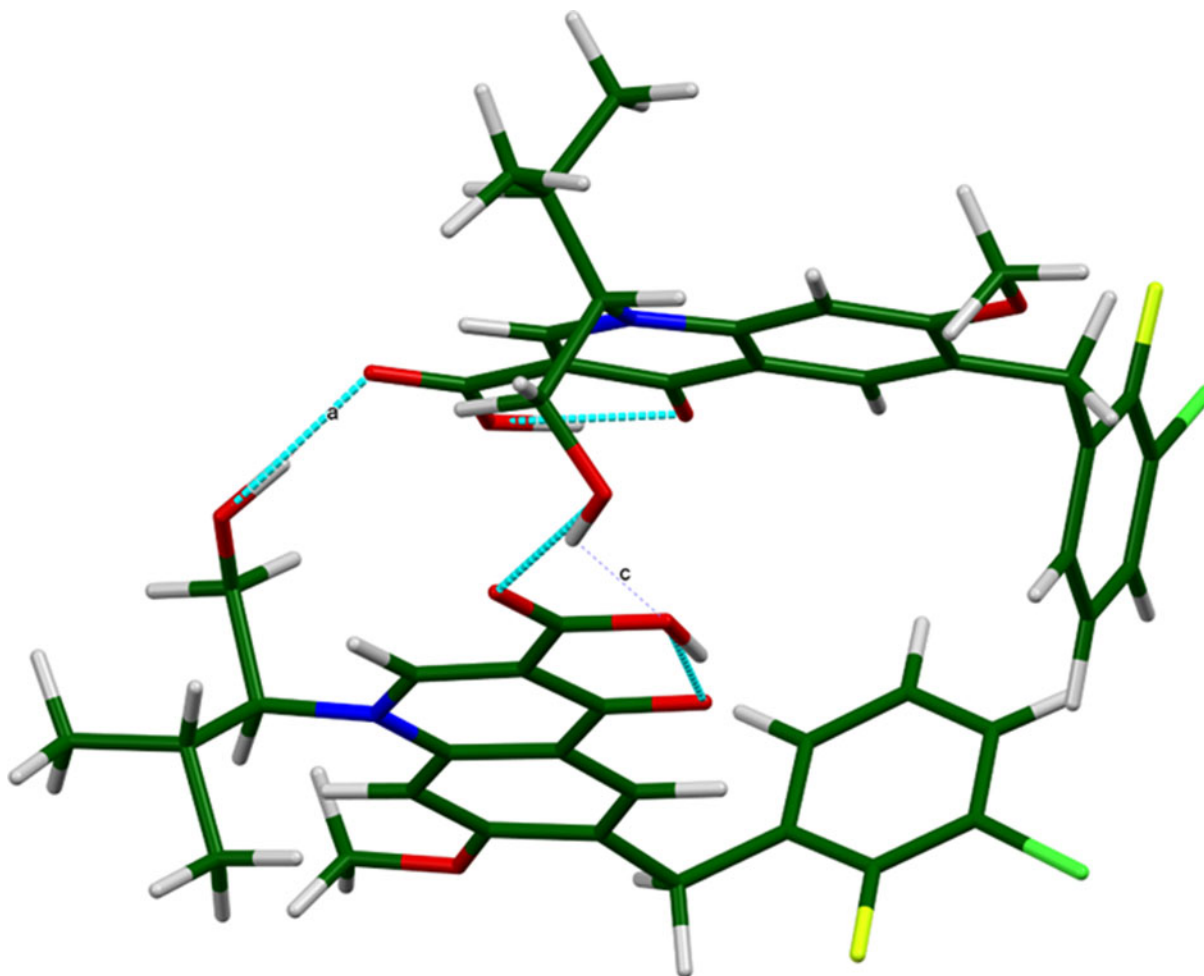


Figure 15. The dimers of elvitegravir, linked by O–H...O hydrogen bonds. Image generated using Mercury (Macrae *et al.*, 2020).

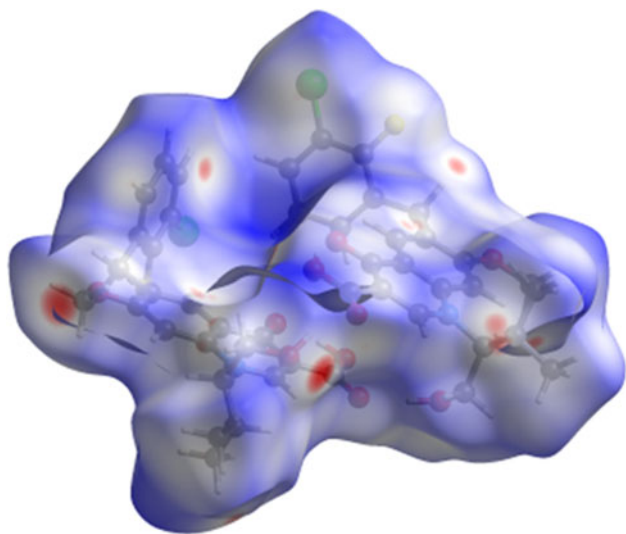


Figure 16. The Hirshfeld surface of elvitegravir. Intermolecular contacts longer than the sums of the van der Waals radii are colored blue, and contacts shorter than the sums of the radii are colored red. Contacts equal to the sums of radii are white. Image generated using CrystalExplorer (Turner *et al.*, 2017).

refinement (including the raw data) and the DFT geometry optimization were deposited with the ICDD. The data can be requested at pdj@icdd.com.

ACKNOWLEDGEMENTS

The use of the Advanced Photon Source at Argonne National Laboratory was supported by the U.S. Department of Energy, Office of Science, Office of Basic Energy Sciences, under Contract No. DE-AC02-06CH11357. This work was partially supported by the International Centre for Diffraction Data. We thank Lynn Ribaud and Saul Lapidus for their assistance in the data collection, and Rebecca Sanders of North Central College for the TGA analysis.

CONFLICT OF INTEREST

The authors have no conflict of interest to declare.

REFERENCES

- Altomare, Angela, Corrado Cuocci, Carmelo Giacovazzo, Anna Moliterni, Rosanna Rizzi, Nicola Corriero, and Aurelia Falcichio. 2013. "EXPO2013: A Kit of Tools for Phasing Crystal Structures from Powder Data." *Journal of Applied Crystallography* 46 (4): 1231–5.
- Antao, Sytle M., Ishmael Hassan, Jun Wang, Peter L. Lee, and Brian H. Toby. 2008. "State-of-the-Art High-Resolution Powder X-Ray Diffraction (HRPXRD) Illustrated with Rietveld Structure Refinement of Quartz, Sodalite, Tremolite, and Meionite." *The Canadian Mineralogist* 46 (6): 1501–9.
- Bernstein, Joel, Raymond E. Davis, Liat Shimon, and Ning-Leh Chang. 1995. "Patterns in Hydrogen Bonding: Functionality and Graph Set Analysis in Crystals." *Angewandte Chemie International Edition in English* 34 (15): 1555–73.
- Bravais, Auguste. 1866. *Etudes Cristallographiques*. Paris, Gauthier-Villars.
- Bruno, Ian J., Jason C. Cole, Magnus Kessler, Jie Luo, WD Sam Motherwell, Lucy H. Purkis, Barry R. Smith, Robin Taylor, Richard I. Cooper, Stephanie E. Harris, and A. Guy Orpen. 2004. "Retrieval of Crystallographically-Derived Molecular Geometry Information."

- Journal of Chemical Information and Computer Sciences* 44 (6): 2133–44.
- Crystal Impact. 2022. Diamond. V. 4.6.8. Crystal Impact - Dr. H. Putz & Dr. K. Brandenburg. Windows.
- Dassault Systèmes and BIOVIA. 2021. *Materials Studio*. Dassault Systèmes and BIOVIA, San Diego, CA.
- David, William I. F., Kenneth Shankland, Jacco van de Streek, Elna Pidcock, W. D. Samuel Motherwell, and Jason C. Cole. 2006. "DASH: A Program for Crystal Structure Determination from Powder Diffraction Data." *Journal of Applied Crystallography* 39 (6): 910–5.
- Donnay, J. D. H., and David Harker. 1937. "A New Law of Crystal Morphology Extending the Law of Bravais." *American Mineralogist: Journal of Earth and Planetary Materials* 22 (5): 446–67.
- Dovesi, Roberto, Alessandro Erba, Roberto Orlando, Claudio M. Zicovich-Wilson, Bartolomeo Civalleri, Lorenzo Maschio, Michel Rérat, Silvia Casassa, Jacopo Baima, Simone Salustro, and Bernard Kirtman. 2018. "Quantum-Mechanical Condensed Matter Simulations with CRYSTAL." *Wiley Interdisciplinary Reviews: Computational Molecular Science* 8 (4): e1360.
- Etter, Margaret C. 1990. "Encoding and Decoding Hydrogen-Bond Patterns of Organic Compounds." *Accounts of Chemical Research* 23 (4): 120–6.
- Favre-Nicolin, Vincent, and Radovan Černý. 2002. "FOX 'Free Objects for Crystallography': A Modular Approach to Ab Initio Structure Determination from Powder Diffraction." *Journal of Applied Crystallography* 35 (6): 734–43.
- Friedel, Georges. 1907. "Etudes sur la loi de Bravais." *Bulletin de Minéralogie* 30 (9): 326–455.
- Gates-Rector, Stacy, and Thomas Blanton. 2019. "The Powder Diffraction File: A Quality Materials Characterization Database." *Powder Diffraction* 34 (4): 352–60.
- Gatti, C., V. R. Saunders, and C. Roetti. 1994. "Crystal Field Effects on the Topological Properties of the Electron Density in Molecular Crystals: The Case of Urea." *The Journal of Chemical Physics* 101 (12): 10686–96.
- Groom, C. R., I. J. Bruno, M. P. Lightfoot, and S. C. Ward. 2016. "The Cambridge Structural Database." *Acta Crystallographica Section B. Structural Science, Crystal Engineering and Materials* 72, 171–9.
- Hirshfeld, Fred L. 1977. "Bonded-atom fragments for describing molecular charge densities." *Theoretica chimica acta* 44 (2): 129–38.
- Kaduk, James A., Cyrus E. Crowder, Kai Zhong, Timothy G. Fawcett, and Matthew R. Suchoemel. 2014. "Crystal Structure of Atomoxetine Hydrochloride (Strattera), C17H22NOCl." *Powder Diffraction* 29 (3): 269–73.
- Kim, Sunghwan, Jie Chen, Tiejun Cheng, Asta Gindulyte, Jia He, Siqian He, Qingliang Li, Benjamin A. Shoemaker, Paul A. Thiessen, Bo Yu, Leonid Zaslavsky, Jian Zhang, and Evan E. Bolton. 2019. "PubChem 2019 Update: Improved Access to Chemical Data." *Nucleic Acids Research* 47 (D1): D1102–9. doi:10.1093/nar/gky1033.
- Kresse, Georg, and Jürgen Furthmüller. 1996. "Efficiency of Ab-Initio Total Energy Calculations for Metals and Semiconductors Using a Plane-Wave Basis Set." *Computational Materials Science* 6 (1): 15–50.
- Lee, Peter L., Deming Shu, Mohan Ramanathan, Curt Preissner, Jun Wang, Mark A. Beno, Robert B. Von Dreele, Lynn Ribaud, Charles Kurtz, Sytle M. Antao, Xuesong Jiao, and Brian H. Toby. 2008. "A Twelve-Analyzer Detector System for High-Resolution Powder Diffraction." *Journal of Synchrotron Radiation* 15 (5): 427–32.
- Louër, D., and A. Boulton. 2007. "Powder Pattern Indexing and the Dichotomy Algorithm." In Deutsche Gesellschaft für Kristallographie (Ed.) *Tenth European Powder Diffraction Conference*, (pp. 191–6). Oldenbourg Wissenschaftsverlag. <https://doi.org/10.1524/9783486992540-030>.
- Macrae, Clare F., Ioana Sovago, Simon J. Cottrell, Peter TA Galek, Patrick McCabe, Elna Pidcock, Michael Platings, Greg P. Shields, Joanna S. Stevens, Matthew Towler, and Peter A. Wood. 2020. "Mercury 4.0: From Visualization to Analysis, Design and Prediction." *Journal of Applied Crystallography* 53 (1): 226–35.
- Materials Design Inc. 2016. *MedeA 2.20.4*. Materials Design Inc., Angel Fire, NM.
- MDI. 2022. *JADE Pro version 8.2*. Materials Data Inc., Livermore, CA, USA.
- Peintinger, Michael F., Daniel Vilela Oliveira, and Thomas Bredow. 2013. "Consistent Gaussian Basis Sets of Triple-Zeta Valence with

- Polarization Quality for Solid-State Calculations.” *Journal of Computational Chemistry* 34 (6): 451–9.
- Rammohan, Alagappa, and James A. Kaduk. 2018. “Crystal Structures of Alkali Metal (Group 1) Citrate Salts.” *Acta Crystallographica Section B Structural Science, Crystal Engineering and Materials* 74 (2): 239–52. [https://doi.org.10.1107/S2052520618002330](https://doi.org/10.1107/S2052520618002330).
- Satoh, Motohide, Hiroshi Kawakami, Yoshiharu Itoh, Hisashi Shinkai, Takahisa Motomura, Hisateru Aramaki, Yuji Matsuzaki, Wataru Watanabe, and Shuichi Wamaki. 2007. “4-Oxoquinoline Compound and Use Thereof as Pharmaceutical Agent.” U.S. Patent 7,176,220, issued February 13, 2007.
- Satoh, Motohide, Takahisa Motomura, Takashi Matsuda, Kentaro Kondo, Koji Ando, Koji Matsuda, Shuji Miyake, and Hideto Uehara. 2009. “Stable Crystal of 4-Oxoquinoline Compound.” U.S. Patent 7,635,704, issued December 22, 2009.
- Shields, Gregory P., Paul R. Raithby, Frank H. Allen, and WD Samuel Motherwell. 2000. “The Assignment and Validation of Metal Oxidation States in the Cambridge Structural Database.” *Acta Crystallographica Section B: Structural Science* 56 (3): 455–65.
- Silk Scientific. 2013. *UN-SCAN-IT 7.0*. Silk Scientific, Orem, UT.
- Sykes, Richard A., Patrick McCabe, Frank H. Allen, Gary M. Battle, Ian J. Bruno, and Peter A. Wood. 2011. “New Software for Statistical Analysis of Cambridge Structural Database Data.” *Journal of Applied Crystallography* 44 (4): 882–6.
- Toby, Brian H., and Robert B. Von Dreele. 2013. “GSAS-II: The Genesis of a Modern Open-Source All Purpose Crystallography Software Package.” *Journal of Applied Crystallography* 46 (2): 544–9.
- Turner, M. J., J. J. McKinnon, S. K. Wolff, D. J. Grimwood, P. R. Spackman, D. Jayatilaka, and M. A. Spackman. 2017. “CrystalExplorer17.” 76730. <http://hirshfeldsurface.net>.
- van de Streek, Jacco, and Marcus A. Neumann. 2014. “Validation of Molecular Crystal Structures from Powder Diffraction Data with Dispersion-Corrected Density Functional Theory (DFT-D).” *Acta Crystallographica. Section B, Structural Science, Crystal Engineering and Materials* 70 (Pt 6): 1020–32.
- Vellanki, Siva Rama Prasad, Vilas Nathu Dhake, Satyanarayana Ravi, Ravi Nuchu, and Ravindra Puliya. 2010. Novel polymorphic forms of elvitegravir and its pharmaceutically acceptable salts. World Intellectual Property Organization WO2010137032A2, filed May 11, 2010, and issued December 2, 2010.
- Wang, Jun, Brian H. Toby, Peter L. Lee, Lynn Ribaud, Sytle M. Antao, Charles Kurtz, Mohan Ramanathan, Robert B. Von Dreele, and Mark A. Beno. 2008. “A Dedicated Powder Diffraction Beamline at the Advanced Photon Source: Commissioning and Early Operational Results.” *Review of Scientific Instruments* 79 (8): 085105.
- Wavefunction, Inc. 2020. “Spartan '18” Version 1.4.5. Wavefunction, Inc., Irvine, CA.